Proceedings of the Twenty-eighth (2018) International Ocean and Polar Engineering Conference **www.isope.org**
Sapporo, Japan, June 10-15, 2018

ISBN 978-1-880653-87-6; ISSN 1098-6189

A Numerical Study of a Freely Floating Lifeboat in Regular Waves

Hao Chen, Ling Qian, Zhihua Ma, Derek Causon and Clive Mingham
School of Computing, Mathematics & Digital Technology
Manchester Metropolitan University, Manchester, UK

ABSTRACT

In the present paper, the open source toolbox OpenFOAM was applied for analysis of the hydrodynamic force and motion of a floating lifeboat in regular waves. The Reynolds averaged Navier-Stokes (RANS) equations were solved and the free surface tracking was achieved by using the volume of fluid method. An overset mesh method was applied for the moving boundary of the lifeboat, in which a body-fitted mesh was generated around the lifeboat using the utility snappyHexMesh and a hexahedral background mesh was produced by the utility blockMesh. The field values were interpolated in the overlapping area between these two layers of meshes. The hydrodynamic forces and the motion of the lifeboat were calculated under the condition that the lifeboat was off-centered in the wave flume to mimic the effects of a larger mother ship. Due to the unsymmetrical condition, full six-degree of freedom (DOF) motion needs to be taken into account. The predicted hydrodynamic force and surface elevation for the fixed lifeboat, and the six DOF motion of the lifeboat were compared to the experimental data. Satisfactory agreement was achieved except the roll moment and motion, for which large discrepancies were observed.

KEY WORDS: lifeboat; hydrodynamics; OpenFOAM; 6 DOF ship motion, overset meshing technique

INTRODUCTION

Lifeboat has been an important component of ocean-going vessels and oil/gas platforms. It needs to be designed to guarantee an effective and safe evacuation for the people on board. Lifeboats can either be dropped freely or lowered via wires. For a freefall lifeboat, it will experience water impact, submergence and resurfacing phases. During the impact phase, the lifeboat may be subjected to high impact loads. However, the advantage of a freefall lifeboat is that it can rapidly reach a safe position and speed suitable for an effective retreat (Ringsberg et al. 2017). The impact loadings on a wired lifeboat could be much lower, but it requires a longer time in the launch process. Essential for both types of lifeboats, after the deployment, they should be able to reach the safe position with acceptable motion amplitudes.

Some recent studies on the impact phase of free-falling lifeboats have been reported in the literature. Mørch (2008) proposed a computational fluid dynamic (CFD) approach to analyse the launching process. Tregde (2015) further considered the compressibility of air to deal with the closed air pocket formed behind the pilothouse and the stern. The numerical results computed by the compressible air model compare very well to the full-scale experimental results. Ringsberg et al. (2017) demonstrates the practical use of quasi-response prediction methods for the assessment of impact loads on modern free fall lifeboats.

RANS simulation has been widely applied for ship hydrodynamic problems, including resistance prediction, seakeeping and manoeuvring analysis. The Gothenburg-Tokyo workshop has been taking place every five years to collect the results of the test cases from different viscous flow codes, and discuss the latest development in the numerical ship hydrodynamics, see e.g. Larsson et al (2013). Besides this, there have been a large number of journal publications on RANS computation of ship hydrodynamics, e.g. Guo et al. (2012), Zou and Larsson (2013), Shen et al (2015). Furthermore, a comprehensive review on this topic has been given in Stern et al. (2013), which covers the state-of-the-art viscous flow solver for ship hydrodynamics and the future trend of the development.

A key factor that should be considered in the ship hydrodynamic simulation is the treatment of moving boundary. Traditionally, Arbitrary Lagrangian-Eulerian (ALE) has been used, e.g. Yang et al. (2017). Alternatively, immersed boundary method can be applied to avoid any deformation of the mesh as in Yang (2017) and Yang et al. (2017). However, it is decided to use the overset mesh in this work, which contains a composite mesh with two or more mesh layers. This technique does not involve any deformation of mesh, nor suffer from spurious pressure oscillations occurred in immersed boundary method. It has been used in Shen et al (2015) for computation of VLKC ship and Ma et al. (2018) for wedge entry problem.

In the present paper, we focus on the motion analysis of the lifeboat in the sailing phase. There are several differences between a lifeboat and a commercial ship in terms of motion analysis. The scale of a lifeboat is much smaller than a commercial ship. Therefore, the diffraction effect is expected to be small. Furthermore, in the initial state of the sailing phase, the lifeboat is in the vicinity of the mother ship. The interaction between the mother ship and the lifeboat should be taken into account. Presently we treat the hull of the mother ship as a wall and assumes that the effect of the mother ship is equivalent to the near wall effect. This is a reasonable assumption considering the distinct scales between a

lifeboat and its mother ship (In many cases the ratio can reach 1:10).

The remainder of the paper is organized as follows. The numerical model is first described, which includes the treatment of free surface flow, rigid body motion and flow turbulence. Then the physical experiments of a lifeboat model in wave flume are briefly introduced, followed by the verification and validation of the numerical model. The obtained numerical results are then carefully analysed through the comparison with the experimental data. Finally the conclusions are given.

THE GOVERNING EQUATIONS

In this paper, we adopted the open source toolbox OpenFOAM, which is based on the collocated finite volume method. It has been widely used in many areas e.g. chemical engineering, combustion modelling, aerodynamics etc. Recently it has also been gaining popularity in coastal and ocean engineering, see e.g. Jacobsen (2012). A specific version of OpenFOAM namely v1706, which provides some new features especially the overset meshing capability, was applied in the present work.

Free surface flow solver

The numerical model solves the incompressible Navier–Stokes equations for a two-phase flow of water and air with incorporation of a VOF scheme for tracking the free surface, which are given by

$$\nabla \cdot u = 0 \tag{1}$$

$$\frac{\partial(\rho u)}{\partial t} + \nabla \cdot (\rho u)u = -\nabla p - (g \cdot x)\nabla \rho + \nabla \cdot \mu(\nabla u) \tag{2}$$

$$\frac{\partial \alpha}{\partial t} + \nabla \cdot u\alpha + \nabla \cdot u_r \alpha(1-\alpha) = 0 \tag{3}$$

where $u=(u, v, w)$ is the velocity field in Cartesian coordinates, and g is the vector of gravity, ρ is density and μ is the effective viscosity which includes both molecular and turbulent viscosity. The dynamic pressure was applied in Eq. 2, where the hydrostatic pressure is subtracted. The total pressure is reconstructed at every time step. Eq. 3 is the transport equation for volume fraction field α. In OpenFOAM an anti-diffusive term is introduced to compress the interface. The velocity field u_r is the so-called compressive velocity field. It is only active at the interfacial area.

Turbulence model

For ship hydrodynamic problems, the flow essentially becomes turbulent. Hereby a turbulence model is needed. Although for this specific problem, the dimension of the lifeboat itself is much smaller than the commercial ships, in many cases the Reynolds number can reach 10^4~10^5 in model scale. Therefore, we applied the commonly used k-ω SST model. This is a blended model, which combines the advantages of k-ω model and k-ε model. Therefore, it is expected to produce reasonable results in both free-shear layer and wall-mounted boundary layer. However, we shall emphasize that the turbulence is not dominant in this problem and instead the free surface effects are the determinant factors given the relatively small KC number.

Ship motion solver

In the numerical model, the hull of the lifeboat was treated as a rigid body. The local and global hull girder deformation under wave condition was neglected. A six-degree of freedom motion solver was natively provided in OpenFOAM, which directly solves the mass and momentum conservation equations. The external forces and moments were collected from integration of the pressure and viscous stress and the mooring forces as follows:

$$F = \iint_S (pn + \tau)dS + F_{Mooring} \tag{4}$$

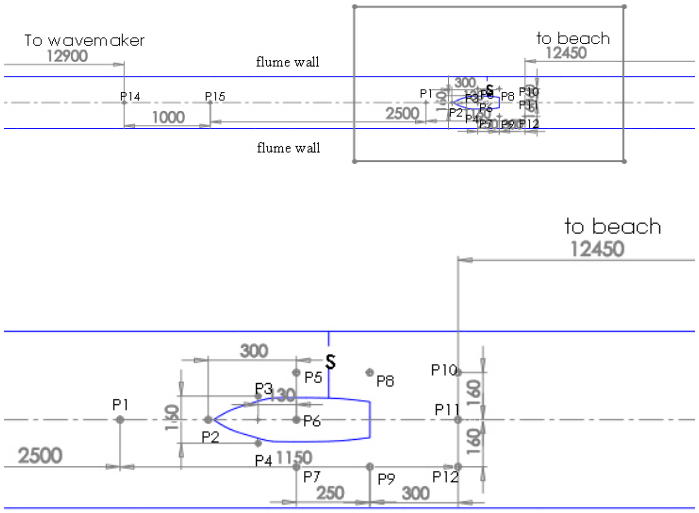

Figure 1. Distribution of the wave gauges in the experiments for fixed lifeboat in the center of the flume. Upper: An overview of the distribution from the wavemaker to the lifeboat. Lower: Zoom in of the upper figure around the lifeboat, which shows the detailed position of wave gauges 1-12.

$$M = \iint_S [r_{CS} \times (pI + \tau)]dS + r_{CM} \times F_{Mooring} \tag{5}$$

where F and M are the external force and moments due to hydrodynamics and moorings. p and τ are the pressure and viscous stress acting on the lifeboat surface. r_{CS} and r_{CM} are the arms of the hydrodynamic and mooring forces, respectively. The Newmark integration scheme was applied to obtain the linear and angular velocity and displacement from the acceleration. Under-relaxation was applied to maintain the stability of the solver.

SETUP OF THE NUMERICAL MODEL

Physical experiments

The physical experiments were performed at COAST Laboratory in Plymouth University, UK. The wave flume has a length of 30 m and width of 0.6 m. The water depth was set to 0.75 m. The lifeboat was downscaled to 1:20 in the experiments, and manufactured with carbon composite. The distance between the wave-maker and the lifeboat was set to 17 m. The length between perpendiculars was 0.5 m for the model scale lifeboat. The beam was 0.149 m and the draft was 0.0535 m. In hydrostatic condition, the lifeboat could keep stable at free surface with the design draft without trim.

Two sets of experiments have been conducted. One was for fixed lifeboat in regular waves, corresponding to the diffraction case. The other was the free-floating lifeboat, where wave radiation was also

involved. For both cases, experiments with centered and off-centered lifeboat have been done. For the case with fixed lifeboat, the hydrodynamic force and moment were measured by a six-axis load cell, which was attached at the position of the center of gravitation. Meanwhile 14 wave gauges were installed around the lifeboat to measure the wave elevation. The position of them for centered lifeboat has been shown in Fig. 1. For the unsymmetrical conditions, the wave gauges were moved with the same distance with the lifeboat, except gauge 1, 14 and 15, which were kept in the same position. Regarding the case with floating lifeboat, the lifeboat was moored at the bow and stern with horizontal linear springs, whose stiffness was 6 N/m. No other constrains were added. Therefore, full six degree of freedom motion was allowed, and they were recorded by the Qualisys tracking system.

Computational domain and mesh

In the present paper, we will reproduce the experiments for both fixed and floating lifeboat, which was positioned off-centered in the wave flume. The separation distance S (see figure 1) from the flume wall to the lifeboat hull is 15 cm, which gives an off-centered distance of 7.5 cm. The incoming wave condition is that the wave height H=0.021 m, wave period T=0.78 s. The numerical model was set up according to the physical experiments described above. A 3D numerical wave tank was applied, which has the same width and water depth as in the experiments. However, the length of the numerical model was shortened as $-10L_{pp}<x<3L_{pp}$, where L_{pp} is the length between perpendicular. The wave was propagating from the right side to the left side in the numerical wave tank. It was generated and absorbed using the active wave boundary conditions presented in Higuera et al. (2013). They have been integrated in OpenFOAM v1706. So the users do not need to download and compile them separately. The surface elevation and the velocity components at the wave generation boundary were calculated based on Stokes second order wave theory, which was selected based on the wave conditions in the simulation. The boundary condition at the bottom of the flume is set to be slip, since we focus on the free-surface hydrodynamics. The top boundary condition was the typical atmosphere boundary condition which applies zero-gradient on all components of the velocity except where there was inflow, in which case a fixed-value condition is applied. The *totalPressure* boundary condition is set for pressure field, where the pressure is adjusted according to the change of velocity.

Overlapping meshes were used in the present work to handle large-amplitude motions effectively without deteriorating the quality of grids. Two (or more) separated meshes, namely a background grid covering the whole domain and a body-fitted grid around the ship hull, were generated. More details on the implementation of overset grid within the framework of OpenFOAM can be found in Ma et al. (2018). By using the *blockMesh* utility in OpenFOAM, a regular hexahedral mesh was generated in the domain as the background mesh. The body-fitted mesh was generated by using the *snappyHexMesh* utility. The geometry of the lifeboat was represented by a stereo lithography surface file. Then the mesh gradually conformed to the surface by iteratively refining a starting mesh and morphing the resulting split-hex mesh to the surface. Near the free surface and the lifeboat, the background mesh was refined to improve the accuracy of numerical calculations as shown in Fig. 2. The grid size in the body-fitted mesh was in general the same as the grid size in the refined area in the background mesh. In the region adjacent to the surface of the lifeboat, the mesh was refined three times as shown in Fig. 3. Fig. 4 gives a close view of the meshes in the overlapping area, which shows a central slice at y=0.

VERIFICATION OF THE NUMERICAL MODEL

Convergence analysis in space and time domain was performed in order to make sure that a reasonable grid size and time step were used in the numerical simulation. Regarding space convergence analysis, grid similarity was required in the convergence analysis. Therefore, we systematically refined the mesh to maximally maintain the grid similarity. Regarding the background mesh, since it was quite regular hexahedral mesh, it was refined simply by increasing the number of grid at each direction. For the body-fitted mesh, the refinement level for the edge and the surface was kept as the same, while the cell size away from the surface was the same as the cell size at the refined area in the background mesh. Table 1 presents the relevant parameters for the mesh used in the convergence analysis. Totally four different meshes were used, and the mesh size was given in Table 1. It should be mentioned that the grid size in x, y and z directions, namely Δx, Δy and Δz are the size at the refined area in the background mesh. At the bottom, the grid size is 8 times larger in x and y direction and 24 times larger in z direction. The cell number given in Table 1 is the total number including both the background mesh and the body-fitted mesh.

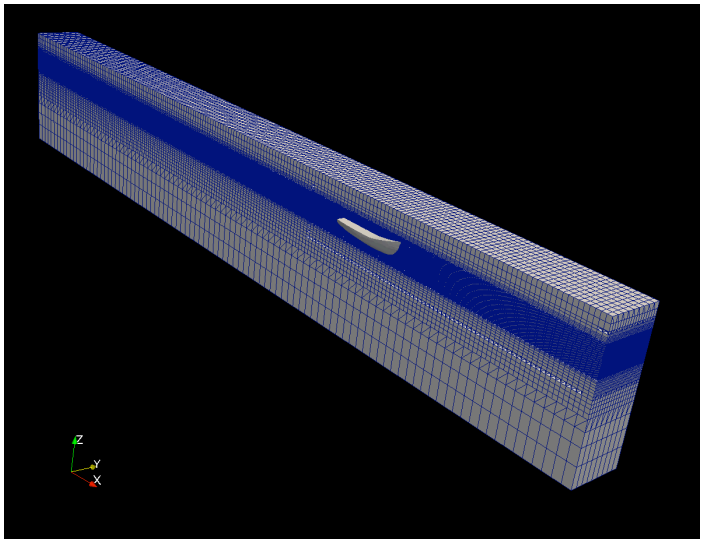

Figure 2. An overview of grid distribution used in the numerical model.

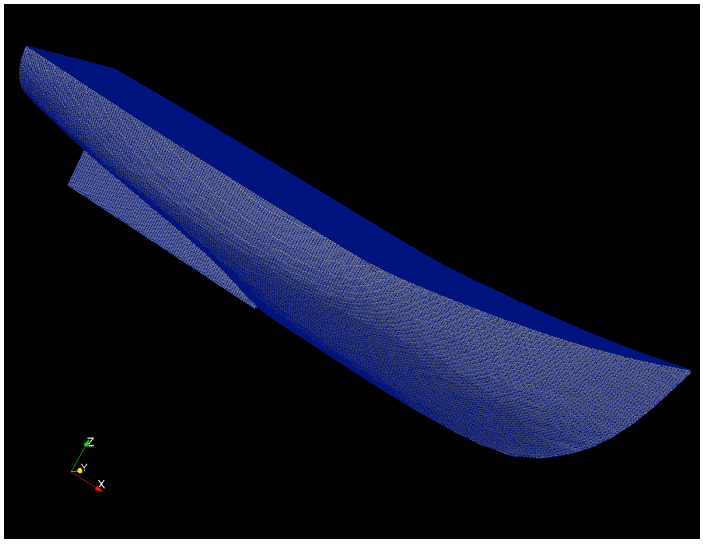

Figure 3. The mesh grid in the lifeboat surface.

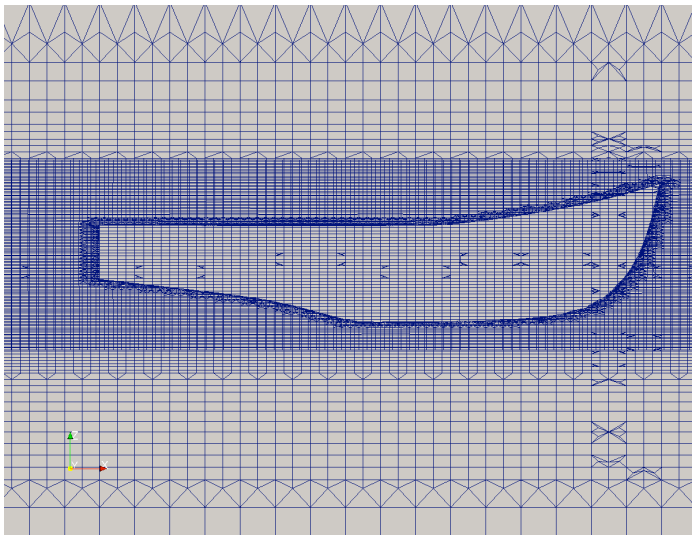

Figure 4. The overlapping of two mesh layers.

Table 1. Mesh parameters for the convergence analysis

Grid level	Δx [m] (background)	Δy [m] (background)	Δz [m] (background)	Cell number
Coarse	0.0108	0.0068	0.0043	639699
Medium	0.0100	0.0063	0.0040	800955
Fine	0.0083	0.0053	0.0033	1394661
Finest	0.0070	0.0044	0.0027	2340491

The results for the grid refinement test is presented in Fig. 5, which output six degree of freedom motion under different grid levels. It is observed that for surge, heave and pitch motion, the convergence behaviour is rather good. The time series of them converges to the same. However, for the other three degree of freedom motion, we are not able to get converged results. For the sway and the yaw motion, we notice that no wave frequency characteristics are presented from the time series of the motion. Furthermore, the absolute value of sway motion is rather small, in the order of 10^{-3}, and the grid resolution is not expected to properly resolve such small motion. Regarding the roll motion, due to unsymmetrical condition, we expect non-zero roll moment due to unsymmetrical diffracted and reflected waves. From the convergence analysis, we notice that the roll motion is not converged with the refinement of the grid levels. The results from the coarsest grid produce the largest roll moment, especially in the first several periods. Meanwhile the fine grid gives smallest roll motion.

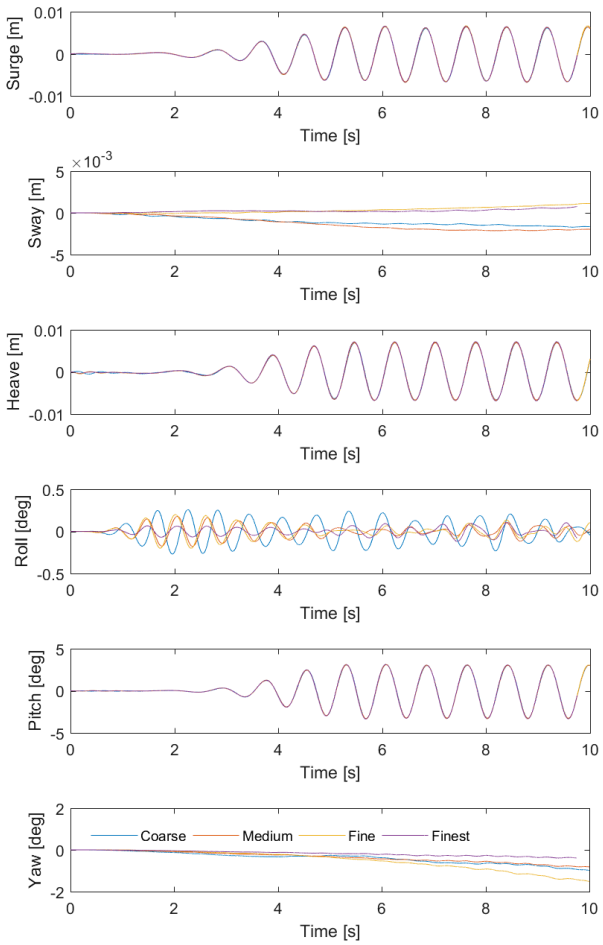

Figure 5. Grid refinement test for the numerical model.

Convergence analysis was also performed by using different time steps. In the numerical simulations, the time step was adjustable based on the Courant number Co. Therefore, in the convergence analysis, the time step was also measured by Courant number. OpenFOAM has introduced a variant of MULES solver, called semi-implicit MULES to solve Eq. 3. This variant of MULES solver can get rid of the stability issues when using large time step, hence no strict constraint on Co was enforced. In the convergence analysis, four different Courant number were tested, namely Co=0.1, Co=0.3, Co=0.5 and Co=1. Fig. 8 presents the motion under different Courant numbers. It is seen that for surge, heave roll and pitch motion, we are able to get a relatively good convergence behaviour. Furthermore, the results from the case with large time step are quite diffusive, which dissipate the energy and reduce the motion amplitudes. This is within our expectations, since we applied first order implicit Euler scheme for time discretization. Numerical diffusion is unavoidable, especially with large time step. This indicates that although stability is ensured using semi-implicit MULES solver, but we may sacrifice the accuracy.

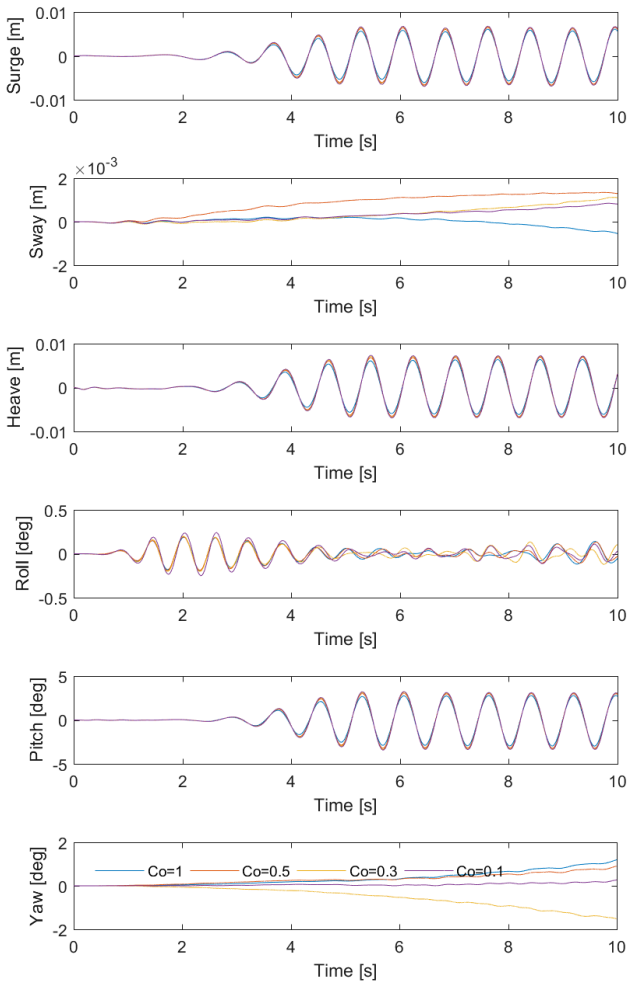

Figure 6. The six-degree of freedom motion under different Courant numbers.

VALIDATION OF THE NUMERICAL MODEL

In this section, the results from the numerical model are compared with the experimental data for both fixed and free floating lifeboat. We applied the results from the case with fine mesh for the validation, and the Courant number was set to 0.25. The computations with this set of parameters were inexpensive. For a 10 s simulation, with 32 CPU cores of Intel-Xeon E5-2600, the computational time was approximately 50 hours. The quantities we focus on in the validation are the hydrodynamic force and the surface elevation for the fixed lifeboat case, and the ship motions for the floating lifeboat case.

Hydrodynamic force

Fig. 7 presents the comparison of the hydrodynamic forces acting on the fixed lifeboat between the numerical model and the experimental data. The surge (Fx), heave (Fz) force and pitch moment (My) are compared quite well with experimental data. For the yaw moment (Mz), the magnitude was predicted slightly larger. Furthermore, from the numerical simulation, the second peak is more obvious than in the experiment. Regarding the transverse load and moment, the numerical model significantly overpredicted them comparing with the experiments. The difference for the transverse load can reach 30%, while for the moment, it is almost 100%.

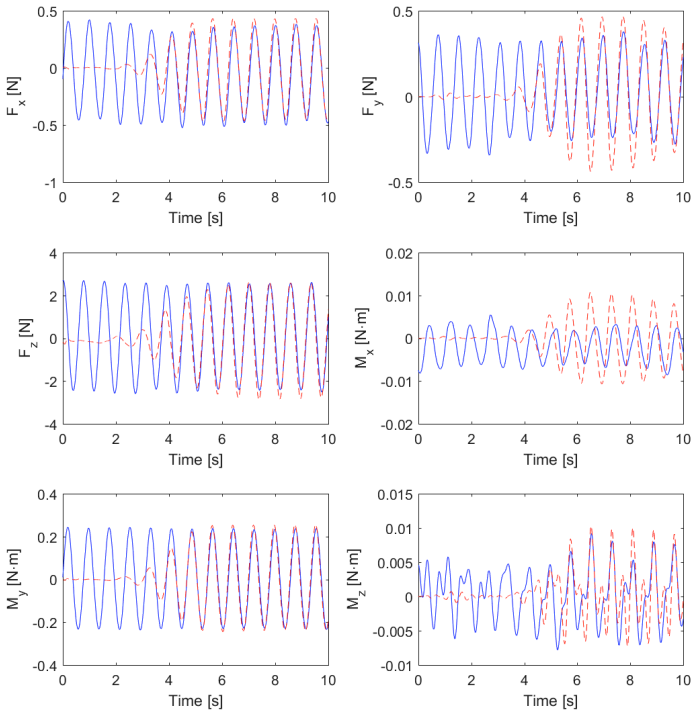

Figure 7. Comparison of the hydrodynamic force on the lifeboat between the numerical model and the experimental data. The solid line is the results from the experiments while the dash line represents the results from the numerical model.

Surface elevation

In this section we compare the surface elevation from wave gauge 01-13, while gauge 05 was deliberately neglected in both experiments and the simulations. The locations of the gauges are shown in Fig. 1, and the results are presented in Fig. 8. In general, the agreement is quite satisfactory for all the wave gauges, although we observe an underestimation of wave trough at e.g. wave gauge 10 and 12. This is probably due to the numerical diffusion. With the propagation of waves, it may dissipate the wave energy, which reduces the amplitude of waves. This essentially becomes more significant in the end of the wave tank.

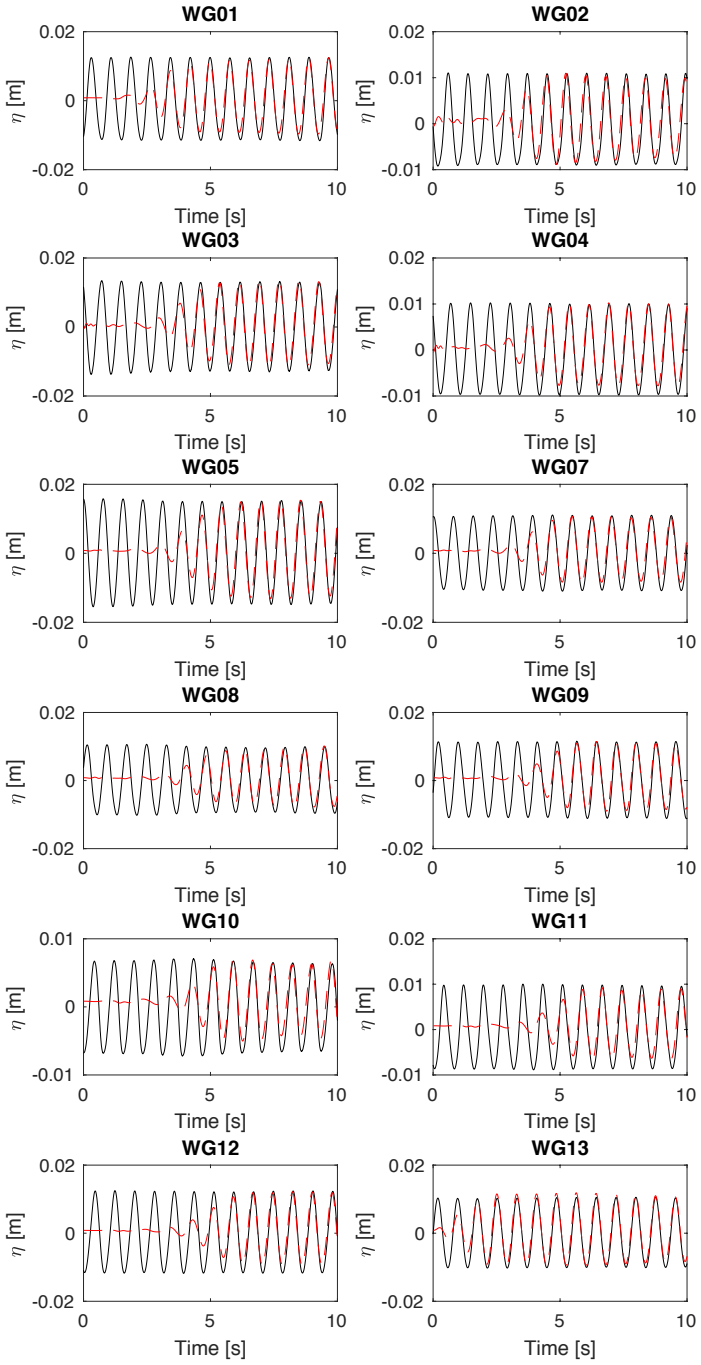

Figure 8. Comparison of the surface elevation between numerical simulation and experimental results for the thirteen wave gauges. The positions of the gauges are given in Fig. 1. The solid line is the results from the experiments while the dash line represents the results from the numerical model.

Ship motion

Fig. 9 presents the comparison of the ship motion from the numerical model and the experiments. Again we notice that we get pretty good agreement for surge, heave and pitch motion. The average error for the first harmonic is less than 10%. The sway motion is in the order of 10^{-3}, which indicates that the unsymmetrical flow condition actually does not have a significant influence on sway motion. For the yaw motion, an steady increase of yaw angle with time was found from the numerical simulation, while for the experiments, it was kept constant. This is also quite grid-sensitive, as for the other level of grid, this is not so significant (see Fig. 5). Grid asymmetry might be a reason. Regarding the roll motion, we notice that it was significantly underestimated by the numerical model, while from Fig. 7, it was concluded that the hydrodynamic force was overestimated. So the moment of inertia might be overestimated. Actually this is an input from the experiments. As the mass was not uniformly distributed, it should be measured from the experiments rather than calculated. Further investigations are needed for the estimation of this parameter. Moreover, we observe a damping of roll motion with propagation of waves from the numerical model. However, in the experiments, the roll motion was amplified. A second peak within one period was also found due to the reflected waves from both sides of the wave flume. This may indicate that the wave diffraction and reflection were not correctly predicted in the numerical wave tank.

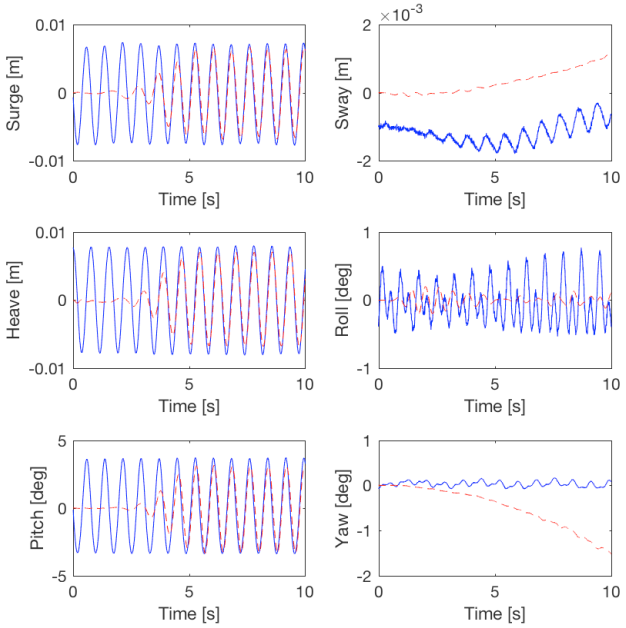

Figure 9. Comparison of the six degree of freedom motion between the results from the numerical model and the experiments. The solid line is the results from the experiments while the dash line represents the results from the numerical model.

Flow field, free surface and vorticity

Fig. 10 presents a few snapshots of the free surface and vorticity contours. With the evolution of the free surface, it is seen that the vorticity was generated near the hull body, and in the wakes. Some vorticities were also observed near the wall, but the strength is not as strong as near the hull. It should also be mentioned that the grid near the hull is finer than the wall. Wall functions were applied on both boundary patches. Typically the maximum y plus value could reach 10 on the hull, while around 80 on the wall. So the vorticity structures near the wall may not be properly resolved. Meanwhile, the vorticity in the streamwise and spanwise direction away from the lifeboat is spurious vorticity due to interpolation between the mesh layers. In reality we shall expect a continuous vorticity field around the lifeboat.

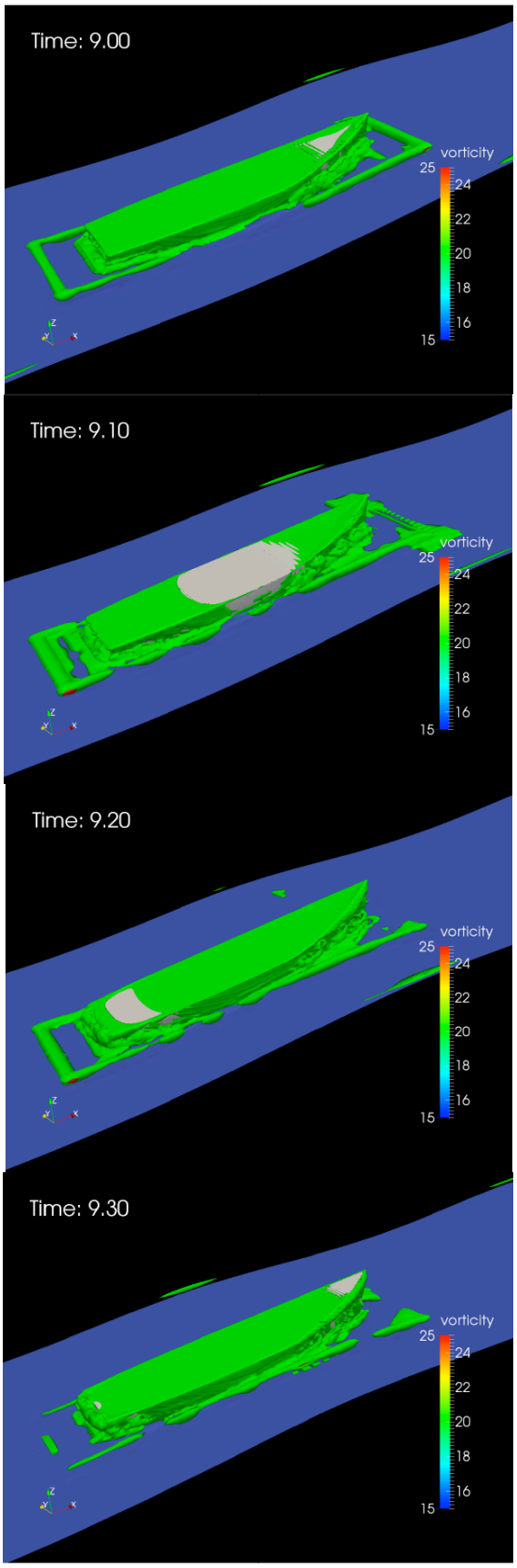

Figure 10. The evolution of free surface and vorticity structures at different time instants. The free surface was indicated by the blue surface.

CONCLUSIONS

This paper presents a numerical simulation of a free floating lifeboat in regular waves. The lifeboat was moored at the bow and stern, and positioned off-cantered in the wave flume. An overlapping mesh based incompressible multiphase flow solver *overInterDyMFoam* released with OpenFOAM-v1706 was applied to deal with the interaction between the lifeboat and waves. For the fixed lifeboat test, attention was focused on the forces on the lifeboat and the surface elevation of the wave when passing through the lifeboat. For the floating lifeboat, the six degree of freedom motion were compared with the experimental data. In general, we found a good agreement for the surge, heave and pitch force/moment and motions. The surface elevation measured around the lifeboat was also predicted well by the numerical model. The deviations are mainly on the roll motion. An overestimation of roll moment was observed, while the roll motion was significantly underestimated. Further investigations are needed on this issue, especially the input roll moment of inertia.

ACKNOWLEDGEMENTS

Dr. Nan Xie from Plymouth University is acknowledged for kindly providing the experimental data. This research was supported by the Engineering and Physical Sciences Research Council (EPSRC), U.K. Project: A Zonal CFD Approach for Fully Nonlinear Simulations of Two Vessels in Launch and Recovery Operations, under Grant No. EP/N008839/1.

REFERENCES

Guo, B. J., Steen, S., Deng, G. B. (2012). Seakeeping prediction of KVLCC2 in head waves with RANS. *Appl Ocean Res*, 35, 56–67.

Higuera, P., Lara, J. L., Losada, I. J. (2013). Realistic wave generation and active wave absorption for Navier-Stokes models. Application to OpenFOAM®. *Coast Eng*, 71, 102–118.

Jacobsen, N. G., Fuhrman, D. R., Fredsoe, J. (2012). A wave generation toolbox for the open-source CFD library: OpenFoam (R). *Int J Numer Methods Fluids*, 70(9), 1073–108.

Larsson L., Stern F., Visonneau M. (2013). CFD in Ship Hydrodynamics—Results of the Gothenburg 2010 Workshop. In: Eça L., Oñate E., García-Espinosa J., Kvamsdal T., Bergan P. (eds) MARINE 2011, IV International Conference on Computational Methods in Marine Engineering. Computational Methods in Applied Sciences, vol 29. Springer, Dordrecht.

Ma, Z. H., Qian, L., Martinez-Ferrer, P. J., Causon, D. M., Mingham, C. G., Bai, W. (2018). An overset mesh based multiphase flow solver for water entry problems. *Comput Fluids*.

Mørch, H. J., Enger, S., Peric, M., Schreck, E. (2008). Simulation of lifeboat launching under storm conditions. In CFD Marin & CD-Adapco, 6th International Conference on CFD in Oil & Gas, Metallurgical and Process Industries, SINTEF/NTNU, Trondheim, Norway.

Ringsberg, J. W., Heggelund, S. E., Lara, P., Jang, B. S., Hirdaris, S. E. (2017). Structural response analysis of slamming impact on free fall lifeboats. *Mar Struct*, 54, 112–12.

Stern, F., Yang, J., Wang, Z., Sadat-Hosseini, H., Mousaviraad, M. (2013). Computational ship hydrodynamics: Nowadays and way forward. *Int Shi Pro*, 60(1–4), 3–105.

Shen, Z., Wan, D., Carrica, P. M. (2015). Dynamic overset grids in OpenFOAM with application to KCS self-propulsion and maneuvering. *Ocean Eng*, 108, 287-306.

Tregde, V. (2015). Compressible Air Effects in CFD Simulations of Free Fall Lifeboat Drop. ASME. *Int Offshore and Polar Eng Conf*, Volume 2: CFD and VIV.

Yang, H., Yan, S., Ma, Q., Lu, J., and Zhou, Y. (2017) Turbulence

modelling and role of compressibility on oil spilling from a damaged double hull tank. *Int. J. Numer. Meth. Fluids*, 83: 841–865.

Yang, L. (2017). One-fluid formulation for fluid–structure interaction with free surface. Computer Methods in Applied Mechanics and Engineering.

Yang, L., Yang, H., Yan, S., & Ma, Q. (2017). Numerical investigation of water-entry problems using IBM method. *Int J Offshore and Polar Eng,* 27(02), 152-159.

Zou, L., Larsson, L. (2013). Computational fluid dynamics (CFD) prediction of bank effects including verification and validation. *J Mar Sci Technol*, 18(3), 310–323.